Rod eutectic growth in bulk undercooled melts

Junfeng Xu[1,3] | Tao Zhang[2] | Peter K. Galenko[3,4]

[1]School of Materials and Chemical Engineering, Xi'an Technological University, 710021, P.R. China

[2]Deakin University, Institute for Frontier Materials, Geelong, Victoria 3216, Australia

[3]Otto Schott Institute of Materials Research, Friedrich-Schiller-University Jena, 07743, Germany

[4]Laboratory of Multi-scale Mathematical Modeling, Department of Theoretical and Mathematical Physics, Ural Federal University, 620000 Ekaterinburg, Russia

Corresponding author. Email address: xujunfeng@mail.nwpu.edu.cn (J.F. XU)

ABSTRACT

This article proposes an analytical model to understand the rod-growth of eutectic in the bulk undercooled melt. Based on the previous derivations of the lamellar eutectic growth models, relaxing the assumptions of small Peclet numbers, the model is derived by considering melt kinetic and thermal undercoolings. The intent of this model is to predict the transitions in eutectic pattern for conditions of the low and high growth velocity. In addition to investigation of the transition between lamellar and rod eutectic pattern, mathematical simplifications of solving Bessel function are presented as well, which is the most important priority to model calculation.

Keywords: Rod eutectic; growth; model; undercooling

MSC CLASSIFICATION

80A22; 82C26

1 INTRODUCTION

Eutectic growth is characterized as two solid phases cooperatively grown from a liquid that is found in most of alloys [1]. The eutectic structures appeared as lamellar or rod-like morphologies, depend on actual solidification conditions[2]. To better understand the eutectic growth, Jackson and Hunt (JH-model) [3] first derived a model for lamellar and rod growth of eutectic in the diffusion-limited condition. Trivedi *et al*. (TMK-model) [4] extended JH-model to the process of rapid solidification.

Kurz and Trivedi [5] further considered the chemical distribution coefficient k as the function of growth velocity instead of its constant value being used in prior models. Later, a model considering the kinetic and thermal undercoolings was established by Li-Zhou *et al.* (LZ-model) [6,7] to depict the anomalous eutectics formed during solidification of undercooled melts. Moreover, Xu *et al.* [8,9] proposed a model attributed the suppression of eutectic decompositions to chemically partitionless solidification at a high growth velocity. Choudhury et al. [10] studied lamellar eutectic three-phase growth in ternary alloys.

As for rod growth of eutectic, the established models consider varied solidification conditions [11-13]. However, these models are basically obtained based on the JH model and using small Peclet numbers. Recently, Trivedi and Wang (TW) [14] relaxed the assumption of small Peclet numbers and obtained a model of rod growth even at high growth rates. However, their derivation is difficult to follow due to, (*i*) incomplete expression of the phase diagrams (i.e., cigar-shape and equal-distribution coefficients, (*ii*) lack of detailed Bessel function calculations [15], and (*iii*) neglect of thermal undercooling. Therefore, to develop a model based on TW and LZ model by addressing the shortcomings of the above-mentioned. Therefore, the present work is to attain this model for rod eutectic growth in bulk undercooled melts, especially at high growth rates.

2 MODEL EQUATIONS

Figure 1a presents a binary alloy system with elements A and B, having the specific eutectic concentration of C_E and equilibrium temperature of T_E. The ΔC_α and ΔC_β represent the concentration differences between phases α, β and eutectic point, respectively. Figure1b schematically illustrates the rod growth of eutectic, which is a kind of regular eutectic with couple growth [3]. The rod phase is denoted as the α-phase with radius r_α, while the matrix is the β-phase.

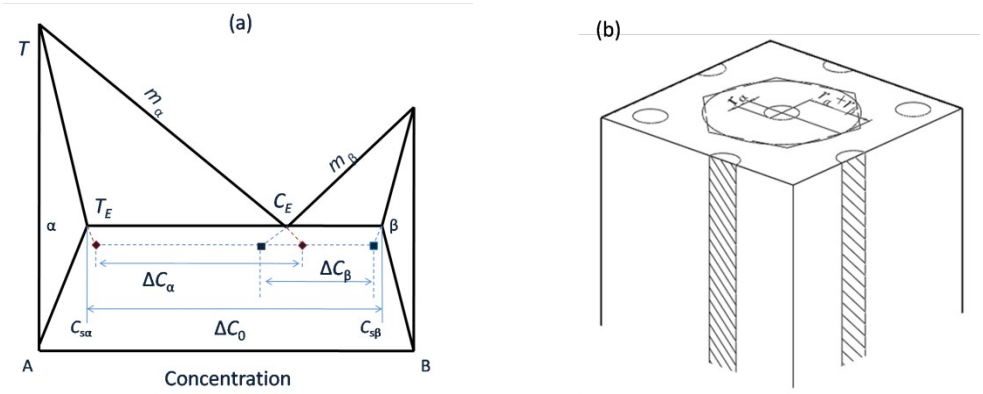

Fig. 1 (a) Eutectic phase diagram, and (b) schemata of a rod eutectic interface viewed normal to the interface.

Following the classical theory, the steady-state diffusion profile in the cylindrical coordinate system is governed by the equation [14]:

$$\left(\frac{\partial^2 C}{\partial r^2}+\frac{1}{r}\frac{\partial C}{\partial r}\right)+\frac{\partial^2 C}{\partial z^2}+\frac{V}{D}\frac{\partial C}{\partial z}=0 \qquad (1)$$

with the boundary conditions given by:

-periodicity: $C(r+R)=C(r)$, here $R=(r_\alpha+r_\beta)$,

-symmetry: $\partial C/\partial r=0$ for $r=0$ and $r=R$,

-far-field: $C=C_\infty$ for $z\rightarrow\infty$,

where C_∞ is the liquid composition far from the interface. The solution of the diffusion equation (1) is obtained as:

$$C = C_\infty + A_0 \exp\left(-\frac{Vz}{D}\right)+\sum_{n=1}^{\infty} A_n J_0\left(\frac{\gamma_n r}{R}\right)\exp\left(-\omega_n z\right) \qquad (2a)$$

where

$$\omega_n = \frac{V}{2D}+\left[\left(\frac{V}{2D}\right)^2+\left(\frac{\gamma_n}{R}\right)^2\right]^{1/2} \qquad (2b)$$

Here A_0 and A_n are the Fourier coefficients, J_0 is the Bessel function of the zero order, Υ_n is the n-th root of Bessel function of first order, i.e. $J_1(\Upsilon_n)=0$. According to the Supporting online materials, Υ_n= 3.144n+0.736 (n= 1,2,3....). The A_0 and A_n are obtained from the condition of solute conservation at the sold/liquid interface [6] as,

-solute balance for α-phase ($0 \le r < r_\alpha$)

$$-D\left(\frac{\partial C}{\partial z}\right)_{z=0} = V(C_{l\alpha} - C_{s\alpha}) = VC(r,0)\left(1-k_\alpha\right) \tag{3a}$$

-solute balance for β-phase ($r_\alpha \le r < r_\alpha + r_\beta$)

$$-D\left(\frac{\partial C}{\partial z}\right)_{z=0} = -V\left(C_{l\beta} - C_{s\beta}\right) = -V\left[1-C(r,0)\right]\left(1-k_\beta\right) \tag{3b}$$

where k_α and k_β are the velocity dependent solute partitioning functions for α-phase and β-phase, respectively, at the interface; $C_{l\alpha}$ and $C_{l\beta}$, $C_{s\alpha}$ and $C_{s\beta}$ are the concentrations of the α-phase and β-phase in the liquid and solid, respectively.

To obtain the solution for A_0 and A_n, we shall follow the treatments of TMK-model with the two special types of phase diagrams [4]. The first case is related to the cigar-shaped phase diagram and the second case is related to the equal distribution coefficients.

Case I: The cigar-shaped phase diagram **[4]**

In this case, the solidus and liquidus are parallel below the eutectic temperature. One obtains $C_{l\alpha}$-$C_{s\alpha}$=ΔC_α=*const*, and $C_{l\beta}$-$C_{s\beta}$=ΔC_β=*const* for any undercooling [8]. Then, Eq. (3) can be written as

$$\left(\frac{\partial C}{\partial z}\right)_{z=0} = \begin{cases} -\dfrac{V}{D}\Delta C_\alpha, 0 \le r < r_\alpha \\ \dfrac{V}{D}\Delta C_\beta, r_\alpha \le r < R \end{cases} \tag{4}$$

Combining Eqs. (2) and (4), the coefficient A_0 and A_n can be thus given from Eq. (4) as

$$A_0 = f_\alpha \Delta C_\alpha - f_\beta \Delta C_\beta \tag{5a}$$

$$A_n = 4\sqrt{f_\alpha}\,\Delta C_0 \frac{J_1\left(\gamma_n \frac{r_\alpha}{R}\right)}{\gamma_n [J_0(\gamma_n)]^2}\left(\frac{1}{\sqrt{1+p_n^2}+1}\right) \tag{5b}$$

where $p_n=2\Upsilon_n/Pe$ and Pe is the Peclet number equals $Pe=V\lambda/2D$, and $\lambda=2R$.

Case II: The diagram with equal distribution coefficients for the two phases **[4]**

For this case , k is an arbitrary constant, but $k_\alpha=k_\beta=k_e$, and $C(r,0)=C_\infty/k$. Then Eq. (3) can be written as

$$\left(\frac{\partial C}{\partial z}\right)_{z=0} = \begin{cases} -\dfrac{V}{D}\dfrac{C_\infty}{k}(1-k), & 0 \le r < r_\alpha \\ \dfrac{V}{D}\dfrac{1-C_\infty}{k}(1-k), & r_\alpha \le r < R \end{cases} \tag{6}$$

Using Eqs. (2) and (6), one arrives at

$$A_0 = \frac{(1-k)}{k}\frac{C_\infty r_\alpha^2 - (1-C_\infty)[(r_\alpha + r_\beta)^2 - r_\alpha^2]}{(r_\alpha + r_\beta)^2}$$

(7a)

$$A_n = 4\sqrt{f_\alpha}\,(1-k)\frac{J_1\left(\gamma_n \frac{r_\alpha}{R}\right)}{\gamma_n [J_0(\gamma_n)]^2}\left[\frac{1}{\sqrt{1+p_n^2}-1+2k}\right] \tag{7b}$$

where C_∞ is the liquid compositions far away from the S/L interface.

For the undercooling calculation, the interfacial average composition in liquid is obtained from the LZ treatment [6]. Using Eq. (2a) and the Fourier coefficient for Cases I and II, the average compositions in the liquid at the interface ahead of the α and the β phases are obtained as

$$\bar{C}_\alpha = C_\infty + A_0 + \frac{4V(r_\alpha + r_\beta)}{D}\Delta C_0 M \tag{8a}$$

$$\bar{C}_\beta = C_\infty + A_0 - \frac{4r_\alpha^2(r_\alpha + r_\beta)}{(r_\alpha + r_\beta)^2 - r_\alpha^2}\frac{V\Delta C_0 M}{D} \tag{8b}$$

where the function M for rod eutectic has two cases expression for the phase diagrams. These are:

Case I: The cigar-shaped phase diagram

$$M = \sum_{n=1}^{\infty} \frac{[J_1(\gamma_n\sqrt{f_\alpha})]^2}{\gamma_n^3[J_0(\gamma_n)]^2}\left[\frac{p_n}{\sqrt{1+p_n^2}+1}\right] \tag{9a}$$

$$M + R\frac{\partial M}{\partial R} = \sum_{n=1}^{\infty} \frac{[J_1(\gamma_n\sqrt{f_\alpha})]^2}{\gamma_n^3[J_0(\gamma_n)]^2}\left[\frac{p_n}{\sqrt{1+p_n^2}+1}\right]^2\frac{p_n}{\sqrt{1+p_n^2}} \tag{9b}$$

Case II: The diagram with equal distribution coefficients for the two phases

$$M = \sum_{n=1}^{\infty} \frac{[J_1(\gamma_n\sqrt{f_\alpha})]^2}{\gamma_n^3[J_0(\gamma_n)]^2}\left[\frac{p_n}{\sqrt{1+p_n^2}-1+2k}\right] \tag{10a}$$

$$M + R\frac{\partial M}{\partial R} = \sum_{n=1}^{\infty} \frac{[J_1(\gamma_n\sqrt{f_\alpha})]^2}{\gamma_n^3[J_0(\gamma_n)]^2}\left[\frac{p_n}{\sqrt{1+p_n^2}-1+2k}\right]^2\frac{p_n}{\sqrt{1+p_n^2}} \tag{10b}$$

Then the interfacial undercooling for each phase can be obtained as:

$$\Delta T_\alpha = m_\alpha^v[\bar{C}_\alpha - C(r,0)] + \frac{2a_\alpha^R}{r_\alpha} + \frac{V}{\mu_\alpha} \tag{11}$$

$$\Delta T_\beta = m_\beta^v\left[C(r,0) - \bar{C}_\beta\right] + \frac{2a_\beta^R r_\alpha}{(r_\alpha + r_\beta)^2 - r_\alpha^2} + \frac{V}{\mu_\beta} \tag{12}$$

Where μ_α and μ_β are the kinetic coefficient; $a_\alpha^R = \Gamma_\alpha^R \sin\theta_\alpha^R$ and $a_\beta^R = \Gamma_\beta^R \sin\theta_\beta^R$, are the Gibbs-Thompson relationship for α and β phases; m_α^v and m_β^v are the liquidus slope dependent on growth velocity, respectively. Given $\Delta T_\alpha = \Delta T_\beta = \Delta T_I$ for eutectic growth, eliminating $C(r,0)$ in Eqs. (11) and (12), the interface undercooling can be obtained as

$$\Delta T_I = m^v \left[\left(Q_0^R R + \frac{1}{\mu} \right) V + \frac{a^R}{R} \right] \tag{13a}$$

$$a^R = 2\sqrt{f_\alpha} \left(\frac{a_\alpha^R}{f_\alpha m_\alpha^v} + \frac{a_\beta^R}{f_\beta m_\beta^v} \right) \tag{13b}$$

$$m^v = \frac{m_\alpha^v m_\beta^v}{m_\alpha^v + m_\beta^v} \tag{13c}$$

$$\mu = \frac{m_\alpha^v m_\beta^v \mu_\alpha \mu_\beta}{m_\alpha^v \mu_\alpha + m_\beta^v \mu_\beta} \tag{13d}$$

For Case I, since $\Delta C_\alpha + \Delta C_\beta = \Delta C_0$, thus it arrives at:

$$Q_0^R = \frac{4\Delta C_0}{f_\beta D} M \tag{13e}$$

For Case II, since $\Delta C_0 = 1-k$:

$$Q_0^R = \frac{4(1-k)}{f_\beta D} M \tag{13f}$$

Similar to the treatment for lamellar eutectic in LZ model [6], considering the thermal undercooling, we have:

$$\Delta T = \Delta T_c + \Delta T_r + \Delta T_k + \Delta T_t = m^v \left[\left(Q_0^R R + \frac{1}{\mu} \right) V + \frac{a^R}{R} \right] + \frac{\Delta H}{C_p} Iv(P_t) \tag{14}$$

where $\Delta H=f_\alpha\Delta H_\alpha+f_\beta\Delta H_\beta$, is the weighted heat of fusion of two eutectic phases and C_p is the specific heat of the liquid, Iv is the Ivantsov function, $Iv(u)=u\exp(u)E_1(u)$, in which $E_1(u)=\int_u^\infty \exp(-v)/v\,dv$ is the first exponential integral function. P_t denotes the thermal Peclet number [8].

To analyze the behaviour of rod spacing R, from the minimum undercooling principle and Eq. (14), we obtained relationship for the rod spacing as a function of velocity [6]:

$$VR^2 = a^R / Q^R \tag{15}$$

For Case I:

$$Q^R = \frac{4\Delta C_0}{f_\beta D}\left(M + R\frac{\partial M}{\partial R}\right) \tag{16a}$$

For Case II:

$$Q^R = \frac{4(1-k)}{f_\beta D}\left(M + R\frac{\partial M}{\partial R}\right) \tag{16b}$$

From Eqs. (14)-(16), the relationship of undercooling and interlamellar ΔT-R can be obtained as

$$\Delta T = m^v \frac{a^R}{R}\left(1+\frac{M}{M+R(\partial M/\partial R)}+\frac{1}{\mu Q^R R}\right)+\frac{\Delta H}{C_p}Iv(P_t) \tag{17}$$

As a result of solutions (14)-(17) together with Eqs. (9) and (10), we can determine the growth velocity V and rod spacing R as functions of the melt undercooling ΔT. Neglecting the effect of thermal undercooling, the system of equations (14)-(17) transforms to the expression ΔT-V-λ previously obtained in TW-model[14], note that $\lambda=2R$ for rod eutectic.

For the present model, the slope of the liquidus line m^v is dependent on the growth velocity. It can be given as [16]:

$$m^{V} = m\{1 + \frac{k_e - k[1 - \ln(k / k_e)]}{1 - k_e}\}, \quad (18)$$

where k is the solute segregation coefficient dependent on the growth velocity:

$$k = \frac{k_e + V / V_{DI}}{1 + V / V_{DI}} \quad (19)$$

where V_{DI} is the diffusion speed at the interface[16].

Using the same parameters of $f_\alpha/C_{s\alpha}/C_{s\beta}/C_E/C_\infty/m_\alpha/m_\beta/T_E/\mu/D_0/E/V_{DI}$=0.25/0.02/0.98/0.74/0.74/450/450/1400/0.01/8.0×10^{-8}/5×10^4/0.5, the growth velocity as the function of undercooling are calculated by JH model[3] and the present model Eq.(17), as shown in Fig. 2a. The results of Eq.(7) is coincident with the JH-model as the undercooling (ΔT) below ~150 K, then showing increasing deviations as ΔT rising until 400 K. This is a consequence of the relaxations of Peclet numbers. The eutectic rod spacing as the function of growth velocity is shown in Fig. 2b, it can found that the rod spacing result from the present model is small than that from JH model.

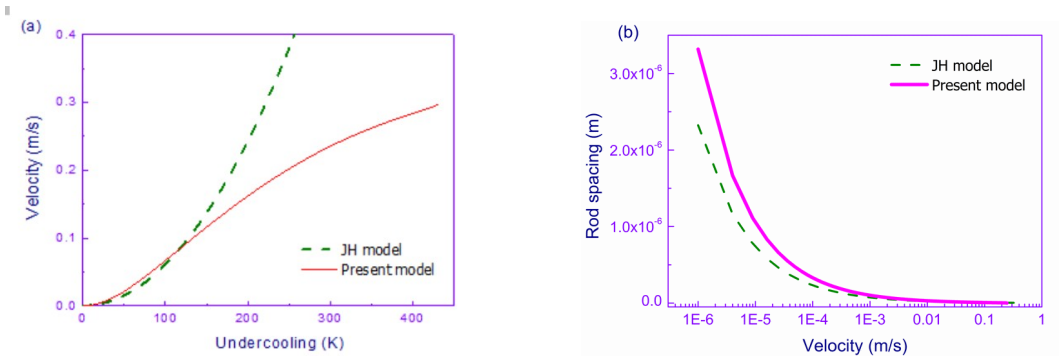

Fig.2 Model calculation of JH model and the present model for different growth velocity: (a)V-ΔT; (b)R-V

Moreover, the present model is approximately identical to the lamellar growth of eutectic as incorporating kinetic and thermal undercoolings upon solidification into the model. To study the phase selection of rod and lamellar eutectic, one needs to figure out the relationship between the growth velocity and undercooling for the two models. For LZ model, the lamellar eutectic growth relation can be given as [6]:

$$\Delta T^{L} = m\left(\frac{\Delta C_0 P}{f_\alpha f_\beta D}\lambda + \frac{1}{\mu}\right)V + m\frac{a^{L}}{\lambda} + \frac{\Delta H}{C_p} Iv(P_t) = f^{L}(V, f_\alpha) \tag{20a}$$

For the present rod eutectic model, the similar form can be written as:

$$\Delta T^{R} = m\left(\frac{4\Delta C_0 M}{f_\beta D}R + \frac{1}{\mu}\right)V + m\frac{a^{R}}{R} + \frac{\Delta H}{C_p} Iv(P_t) = f^{R}(V, f_\alpha) \tag{20b}$$

As is known, if several structures compete at a given growth rate, the structure that requires the lowest ΔTwill grow preferentially. Thereafter, if we calculate ΔT via Eq. (20)at a fixed growth velocity and variation of f_α, it is possible to predict structural preference in normal eutectic growth. The lowest ΔT corresponds to the winning growth mode. Thus, we use a group calculation to show the transition in between the rod and lamellar eutectic.

Using Eq.(20) with Case I phase diagram expressions and parameters of $C_{s\alpha}/C_{s\beta}/m_\alpha/m_\beta/k_\alpha/k_\beta/V_{DI}/T_E/\mu/D_0/E$=0.02/0.98/450/450/0.0226/0.1724/0.5/1400/0.01/8.0×10^{-8}/5×10^4, the relationship of ΔT-V-$\lambda(R)$ is given as shown in Fig.3a. It can be found that the surface diagram of $\Delta T^{R}=f^{R}(V,f_\alpha)$ and $\Delta T^{N}=f^{L}(V,f_\alpha)$ have a common line of intersection at about f_α=0.2~0.35, which is corresponding to critical fraction values $f_\alpha^{*}$for the rod-lamellar eutectic transition at different V. At a constant V, if $f_\alpha<f_\alpha^{*}$, the undercooling of rod eutectic is lower, so the alloy solidifies with rod eutectic structure; instead, if $f_\alpha<f_\alpha^{*}$, the alloy solidifies with normal lamellar eutectic structure.

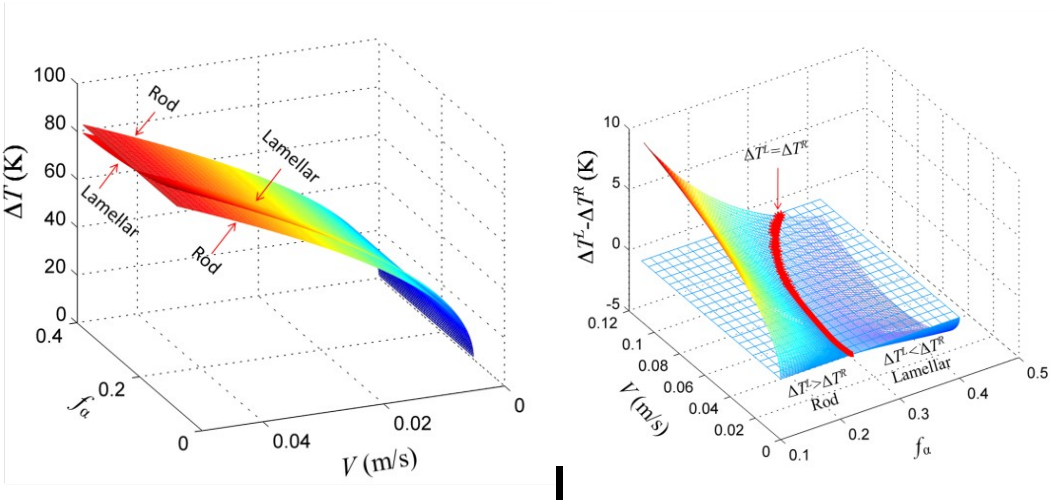

Fig. 3 The calculation result of rod eutectic model and lamellar eutectic model: (a) the surface diagram of $\Delta T^R=f^R(V,f_\alpha)$ and $\Delta T^L=f^L(V,f_\alpha)$; (b) the surface diagram of ΔT^R-ΔT^L change with V and f_α.

From the above description, the one with the same growth velocity and low ΔT wins. Compare Eq. (20a) (LZ model) with Eq. (20b) (present model), the kinetic and thermal undercoolings expressions are totally same, subtracting the two equations thereby leading to,

$$\Delta T^L-\Delta T^R=m\left(\frac{\Delta C_0 P}{f_\alpha f_\beta D}\lambda-\frac{4\Delta C_0 M}{f_\beta D}R\right)V+m\left(\frac{a^L}{\lambda}-\frac{a^R}{R}\right)=f(V,f_\alpha) \tag{21}$$

Thus, the critical fraction $f_\alpha^*$for rod-lamellar transition can also be found by plotting $\Delta T^L-\Delta T^R=f(V,f_\alpha)$, as shown in Fig. 3b. The red line is the position when $f(V,f_\alpha)$=0, which represents the critical fraction value f_α^* at varying V. When f_α is larger than f_α^*, there is $\Delta T^L>\Delta T^R\Delta T^R$, so the rod eutectic win in the final structure; on the opposite, the lamellar structure will form. It‘s worth noting that the critical fraction f_α^* increases from 0.2 to 0.35 with increase of growth velocity, which is consistent with Lei's predictions [17]. It indicates that the rod-lamellar transition is dependent on both α-phase fraction and the eutectic growth velocity.

Equations (9), (10), (13), (16) include the function M, which is determined by Bessel function $J_1(\Upsilon_n)$.

The series expansions for Bessel function are expressed as following [18],

$$J_0(x)=\sum_{m=0}^{\infty}\frac{(-1)^m}{(m!)^2}\left(\frac{x}{2}\right)^{2m} \tag{22a}$$

$$J_1(x)=\sum_{m=0}^{\infty}\frac{(-1)^m}{m!(m+1)!}\left(\frac{x}{2}\right)^{2m+1} \tag{22b}$$

Accordingly, it is difficult to solve Eq. (22) as it’s not easy to obtain the boot of equation $J_1(x)$=0, i.e. the values of Υ_n. As the 'Υ_n approximately equal to $n\pi$' by Jackson [3], which was also widely used by

other models [12,13]. Using computer program, we obtain the result Υ_n as calculating the boot of $J_1(x)=0$ by Eq. (22b) for n=1,2,3... 20, as:

Υ_n=[3.83170597020751, 7.01558666981562, 10.1734681350627, 13.3236919363142, 16.4706300508776, 19.6158585104682, 22.7600843805928, 25.9036720876184, 29.0468285349169, 32.1896799109744, 35.3323075500839, 38.4747662347716, 41.6170942128145, 44.7593189976528, 47.9014608871855, 51.0435351835715, 54.1855536410613, 57.3275254379010, 60.4694578453475, 63.6113566984812].

The calculated results are shown in Fig. 4a. It can be seen that the calculated Υ_n are larger than those given by Jackson et. al [3] model, but they are approximately equal to those shown in the Handbook [15]. By fitting with calculated values, we obtianed Υ_n=3.144n+0.736(n=1,2,3....). This easily facilitates the calculations for equations related to the Bessel function, such as the M value in JH model:

$$M_{JH} = \frac{[J_1(\gamma_n\sqrt{f_\alpha})]^2}{\gamma_n^3[J_0(\gamma_n)]^2} = \frac{[J_1[(3.144n+0.736)\sqrt{f_\alpha}]^2}{(3.144n+0.736)^3[J_0(3.144n+0.736)]^2} \qquad (23)$$

In the present study, Eqs. (2), (5), (7), (9), (10) can be easy calculated by Eq. (23)treatment.

Figure 4bpresents the M of JH model ($= \sum_{n=1}^{\infty} \frac{[J_1(\gamma_n\sqrt{f_\alpha})]^2}{\gamma_n^3[J_0(\gamma_n)]^2}$) as function of α phase fraction. It can be found that M value from Υ_n=3.144n+0.736 (n=1,2,3...) is nearly the same to that from Table I in Ref. [3]. However, if $\Upsilon_n \sim n\pi$ is used, the results are deviated from the true value by more than twice (Fig.4b). This further suggests using Υ_n=3.144n+0.736 for Bessel functionin the rod eutectic growth model (that is more accurately than $\Upsilon_n \sim n\pi$).

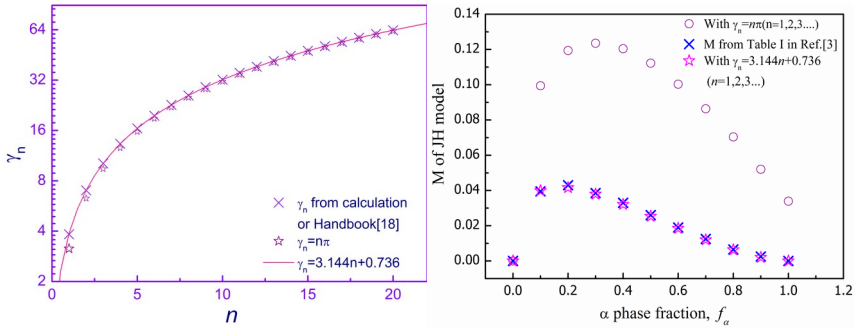

Fig. 4(a) The Υ_n values from different methods; (b) M of JH model ($= \sum_{n=1}^{\infty} \frac{[J_1(\gamma_n \sqrt{f_\alpha})]^2}{\gamma_n^3 [J_0(\gamma_n)]^2}$) calculated with different expression of γ_n values

3 CONCLUSIONS

By relaxing the small Pélect number assumptions, the rod eutectic growth model is developed for the growth velocity and inter rod spacing by considering the kinetic and thermal undercooling in bulk undercooled melts. A simple expression for the equation related to Bessel function is given and the boot Υ_n=3.144n+0.736 (n=1, 2, 3...) is found for Bessel function $J_1(x)$=0, which can also simplify the calculation of the other rod eutectic models. The rod-lamellar eutectic transition has been calculated by combining LZ model and the present model. It shows that the critical phase fraction (about f_α^*=0.2-0.35 here) increases with growth velocity. The developed model can be further extended to the eutectic solidification under local non-equilibrium conditions in the diffusion field as it has been formulated and summarized in Ref. [19].

ACKNOWLEDGEMENTS

This work was supported by the Science and Technology Program of Shaanxi Province (No. 2016KJXX-87) and the Foundation of Shaanxi Provincial Department of Education (No. 18JS050).P.K.G. acknowledges financial support of German Science Foundation(DFG- Deutsche Forschungsgemeinschaft) under the Project GA 1142/11-1. The authors thank JT Cao and AL Bao for their help in this work.

References

[1] Kurz W, Sahm P R. Gerichtet erstarrte eutektische Werkstoffe, Springer Berlin, 1975.

[2] Trepczyńska-ent M. The Criterion of Minimum Entropy Production in Eutectic Growth. *Archives of Foundry Engineering*.2012, 12: 85-88.DOI: 10.2478/v10266-012-0042-9

[3] Jackson KA, Hunt JD. Lamellar and rod eutectic growth.*TMS of AIME*. 1966;236:1129-1142. DOI: https://doi.org/10.1016/B978-0-08-092523-3.50040-X.

[4] Trivedi R, Magnin P, Kurz W. Theory of eutectic growth under rapid solidification conditions. *Acta Metall*. 1987, 35(4):971-980. DOI: https://doi.org/10.1016/0001-6160(87)90176-3.

[5] KurzW, TrivediR. Eutectic growth under rapid solidification conditions. *Metall Trans A*. 1991; 22(12):3051-3057. DOI:https://doi.org/10.1007/BF02650266.

[6] Li JF, Zhou YH. Eutectic growth in bulk undercooled melts. *Acta Mater.*2005; 53(8): 2351-2359. DOI: https://doi.org/10.1016/j.actamat.2005.01.042..

[7] Wei XX, Lin X, Xu W, Huang QS, Ferry M, Li JF, Zhou YH. Remelting-induced anomalous eutectic formation during solidification of deeply undercooled eutectic alloy melts. *Acta Mater*. 2015;95:44-56.DOI:http://dx.doi.org/10.1016/j.actamat.2015.05.014

[8] Xu J, Galenko PK. Effects of local nonequilibrium in rapid eutectic solidification—Part1: Statement of the problem and general solution. *Math. Meth. Appl. Sci*, 2020: 1-10.DOI:10.1002/mma.6960.

[9] Xu J, Rettenmayr M, Galenko PK. Effects of local non-equilibrium in rapid eutectic solidification —Part 2: analysis of effects and comparison to experiment. *Math. Meth. Appl. Sci.*, 2020:1-12. DOI: 10.1002/mma.7004.

[10] Choudhury A, Plapp M, Nestler B. Theoretical and numerical study of lamellar eutectic three-phase growth in ternary alloys, *Physical Review E* 2011, 83: 051608-1-20. DOI: 10.1103/PhysRevE.83.051608.

[11] Caram R, Chandrasekhar S, Wilcox WR. Influence of convection on rod spacing of eutectics. *J Cryst Growth*, 1990, 106: 294-302. DOI: 10.1016/0022-0248(90)90075-V.

[12] Liu S, Lee JH, Trivedi R. Dynamic effects in the lamellar–rod eutectic transition. *Acta Mater*, 2011, 59: 3102-3115.DOI: 10.1016/j.actamat.2011.01.050

[13] Meng GH, Xie H, Lin X. Estimation of rod-like phase spacing in melt-grown eutectic composites. *Science China*,2014,57: 1794-1801.. DOI: 10.1007/s11431-014-5608-z

[14] Trivedi R, Wang N. Theory of rod eutectic growth under far-from-equilibrium conditions: nanoscale spacing and transition to glass. *Acta Mater*. 2012, 60: 3140-3152. DOI: 10.1016/j.actamat.2012.02.020.

[15] Arfken G. "Bessel Functions of the First Kind, Jv(x)" and "Orthogonality." §11.1 and 11.2 in Mathematical Methods for Physicists, 3rd ed. Orlando FL: Academic Press, 1985 pp. 573-591 and 591-596.

[16] Aziz M. Model for solute redistribution during rapid solidification. *J. Appl. Phys*. 1982, 53: 1158-1168.DOI: 10.1063/1.329867.

[17] Wang L, Wang N. Ji L. Yao WJ. "Lamellar↔rod" transition mechanism under high growth velocity condition.*Acta Phys. Sin*. 2013,62:216801-1-7.DOI: 10.7498/aps.62.216801

[18] Abramowitz M, Stegun IA, (Eds.). "Bessel Functions J and Y." §9.1 in Handbook of Mathematical Functions with Formulas, Graphs, and Mathematical Tables, 9th printing. New York: Dover, 1972, pp. 358-364.

[19] Galenko PK, Jou D. *Physics Reports*, 2019, 818: 1-70. DOI: https://doi.org/10.1016/j.physrep.2019.06.002.

Figure captions

Fig. 1 (a) Eutectic phase diagram, and (b) schemata of a rod eutectic interface viewed normal to the interface.

Fig.2 Model calculation of JH model and the present model for different growth velocity: (a) V-ΔT; (b) R-V

Fig. 3 The calculation result of rod eutectic model and lamellar eutectic model: (a) the surface diagram of $\Delta T^{R}=f^{R}(V,f_{\alpha})$ and $\Delta T^{L}=f^{L}(V,f_{\alpha})$; (b) the surface diagram of $\Delta T^{R}-\Delta T^{L}$ change with V and f_{α}.

Fig. 4 (a)The γ_n values from different methods; (b) M of JH model ($= \sum_{n=1}^{\infty} \frac{[J_1(\gamma_n \sqrt{f_\alpha})]^2}{\gamma_n^3 [J_0(\gamma_n)]^2}$) calculated with different expression of γ_n values

Authorship

Authors contributed equally to the content of the manuscript.